CHEMNANOMAT

CHEMISTRY OF NANOMATERIALS FOR ENERGY, BIOLOGY AND MORE

www.chemnanomat.org

Accepted Article

Title: Self-assembly of clicked star-shaped triazines into functional nanostructures

Authors: Martín Castillo-Vallés, Eduardo Beltrán, Jesús Cerdá, Juan Aragó, Pilar Romero, José Luis Serrano, Enrique Ortí, Raquel Giménez, and Teresa Sierra

To be cited as: *ChemNanoMat* 10.1002/cnma.201800484

Link to VoR: http://dx.doi.org/10.1002/cnma.201800484

A Journal of

ACES Asian Chemical Editorial Society

A sister journal of **Chemistry – An Asian Journal** and **Asian Journal of Organic Chemistry**

WILEY-VCH

WILEY-VCH

DOI: 10.1002/ ((please add manuscript number))
Article type: Full Paper

Self-assembly of clicked star-shaped triazines into functional nanostructures

Martín Castillo-Vallés, Eduardo Beltrán, Jesús Cerdá, Juan Aragó, Pilar Romero, José Luis Serrano, Enrique Ortí Raquel Giménez* and Teresa Sierra**

M. Castillo-Vallés, Dr. E. Beltrán, Dr. P. Romero, Prof. J. L. Serrano, Dr. R. Giménez and Dr. T. Sierra
Departamento de Química Orgánica, Instituto de Ciencia de Materiales de Aragón (ICMA)
Universidad de Zaragoza - CSIC
50009 Zaragoza, Spain
E-mail: rgimenez@unizar.es, tsierra@unizar.es

Dr. E. Beltrán
Present address: Merck Chemicals Ltd., University Parkway, Southampton SO16 7QD, UK

J. Cerdá, Dr. J. Aragó, Prof. E. Ortí
Instituto de Ciencia Molecular
Universidad de Valencia
E-mail: enrique.orti@uv.es

Keywords: self-assembly, triazine, nanoparticle, nanotube, AIE

Abstract: Two non-amphiphilic star-shaped 2,4,6-tris(1,2,3-triazol-4-yl)-1,3,5-triazines showing different behavior in terms of self-assembly and luminescent properties are described. They aggregate in the liquid phase to form low-dimensional nanostructures with a variety of morphologies, such as spherical particles, one-hole hollow spheres, toroids, twisted fibers or helical nanotubes, just by varying the conditions of a straightforward reprecipitation method. Aggregation has an opposite effect concerning the fluorescent properties of the proposed compounds, either causing the enhancement or the quenching of the emission after the self-assembly. Quantum chemical calculations have been also performed to assist in the structural and electronic characterization of the two star-shaped compounds.

WILEY-VCH

1. Introduction

In recent years, nanomaterials have aroused great interest due to their unique properties in comparison with their macroscopic counterparts. Organic nanomaterials hold some advantages such as a great variety of chemical structures, low processing costs and tuneable electronic and optical properties, that make them interesting for technological applications.[1–4] Indeed, nanoaggregates made of π-conjugated organic molecules are being investigated as non-linear optical materials,[5,6] fluorescence probes,[7] semiconductors[8] or solar cell dyes.[9]

Organic nanomaterials are usually prepared by bottom-up approaches that involve the self-assembly of small organic molecules in a surrounding media driven by intermolecular interactions, namely, hydrogen bonding, π–π stacking and electrostatic and hydrophilic-hydrophobic interactions, and are able to exhibit different morphologies with low dimensionality such as nanoparticles, nanofibers, nanorods, nanotubes and others. Size and shape of the nanomaterials strongly affect their properties,[10–12] therefore, there is a great interest in controlling their morphology. When dealing with fluorescent organic nanomaterials, avoiding the decrease in emission efficiency that many π-conjugated molecules undergo due to aggregation (or concentration) quenching is a difficult challenge. Indeed, efforts are being focused on the study of molecules that show the opposite effect; that is, molecules that barely emit in liquid solution, but are highly luminescent in the solid state.[13,14] Methods to obtain fluorescent organic nanostructures[15,16] have been achieved from molecules that show the abnormal aggregation-induced enhancement of emission (AIEE)[17] or aggregation-induced emission (AIE) phenomena.[18–20] Recently, the term solid-state luminescence enhancement (SLE)[21] has been proposed to subsume more precisely both the AIEE and AIE terms.

Fluorescent compounds based on the star-shaped 2,4,6-tris(1,2,3-triazol-4-yl)-1,3,5-triazine (TTT) moiety have been widely studied in our group. They are readily prepared by a copper-catalyzed alkyne-azide coupling (CuAAC) click reaction and display promising properties in the field of functional materials due to their liquid crystal, fluorescence and electronic properties.[22,23] The formation of well-organized columnar mesophases is highly favored when the TTT moiety is adequately functionalized at the periphery.[24] The TTT moiety can indeed be used as a core for H-bonded supramolecular liquid crystals,[25] leading to a modular approach to columnar mesophases that makes possible the design of ambipolar charge-transporting materials.[26] Some TTT and other similar triazine derivatives have shown attractive behaviors not only in the bulk, but also in solution, showing to be able to self-aggregate in different solvents.[25,27] This prompted us to investigate the self-assembly of TTT-based derivatives in the liquid phase, how to control the morphology of the aggregates and the consequences that the formation of the aggregates has on their optical properties. The TTT derivatives **T3C$_4$** and **TB3C$_4$** (Scheme 1), with aromatic triazine, triazole and phenyl rings, were foreseen as self-assembling moieties that can aggregate through intermolecular π–π interactions in the appropriate solvent.

We describe herein the preparation of nanostructures with different morphologies and properties of the star-shaped **T3C$_4$** and **TB3C$_4$** TTT derivatives with terminal butoxy chains, which behave differently in their self-assembly and their fluorescent properties. The aggregates were prepared by employing a reprecipitation method using two solvent/non-solvent pairs at different ratios, giving rise to various remarkable morphologies with a significant impact on the optical behavior. Quantum-chemical calculations were also performed to gain insight into the aggregation and optical properties.

WILEY-VCH

2. Results and Discussion

2.1. Synthesis

Compounds **T3C4** and **TB3C4** were both prepared following a previously described "one-pot" procedure.[22] This consists on a CuAAC click reaction that uses as reagents 2,4,6-tris[(trimethylsilyl)ethynyl]-1,3,5-triazine and the corresponding azides, 1-azido-4-butoxybenzene or 4-azidophenyl 4-butoxybenzoate (**1**), occurring in situ the triply removal of the trimethylsilyl groups from the alkyne molecule and the coupling with the azides (Scheme 1). The synthesis of **T3C4** was previously reported,[25] whereas **TB3C4** is a novel compound that has been synthesized by adapting a procedure described in a previous work.[23] In the latter case, the azide intermediate **1** was obtained through a Steglich coupling between 4-azidophenol and 4-butoxybenzoic acid. In turn, 4-azidophenol was prepared by diazotization of 4-aminophenol and subsequent reaction with sodium azide (See the Supporting Information).[28] Thanks to the versatility of the synthetic procedure, the two TTT derivatives incorporate two different structures linked to the triazole ring, **T3C4** with three *p*-butoxyphenyl groups attached to the TTT core, and **TB3C4** with three *p*-butoxybenzoyloxyphenyl groups.

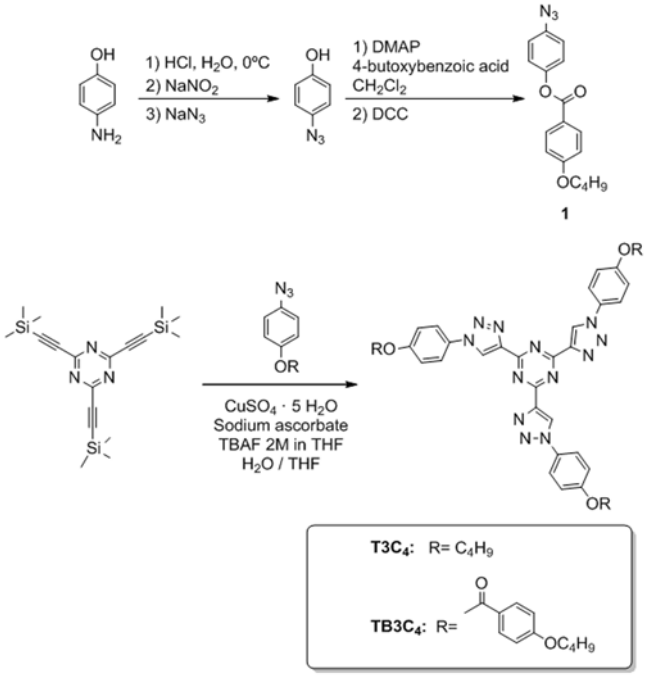

WILEY-VCH

Scheme 1. Synthesis of **T3C4** and **TB3C4**.

2.2. Computational insight into the self-assembly of T3C4 and TB3C4

To investigate the relationship between the molecular structure of **T3C4** and **TB3C4** and their self-assembly tendencies, supramolecular aggregates of both compounds were built and calculated at different quantum-chemical levels. The molecular geometries of the **T3C4** and **TB3C4** monomers were first optimized within C_3-symmetry constrains at the B3LYP-D3/6-31G** level. The minimum-energy structures optimized for both **T3C4** and **TB3C4** exhibit mostly planar conjugated cores, formed by the triazine and the triazole rings (the TTT core), with dihedral angles D_1 of around 1° (Figure 1). The butoxyphenyl peripheral groups of **T3C4** are notably twisted with respect to the triazole rings with dihedral angles D_2 of 29°. For **TB3C4**, the inner benzene rings are twisted by around 26° with respect to the triazoles (dihedral angle D_2) similarly to **T3C4**, and the terminal benzoyloxy groups are additionally rotated with a dihedral angle D_3 of around 44° (Figure 1). The rotation between the inner benzene and the benzoyloxy unit comes from the single character of the carbon–oxygen bond between both moieties. This rotation plays an important role in determining the optical properties of **TB3C4** aggregates (*vide infra*).

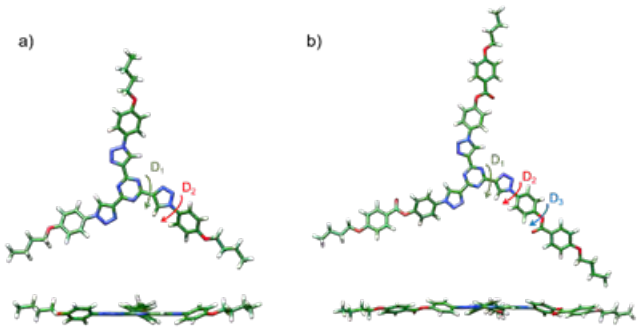

Figure 1. Top and side views of the B3LYP-D3/6-31G**-optimized structures calculated for **T3C4** (a) and **TB3C4** (b). Representative dihedral angles (D_1, D_2 and D_3) are highlighted.

Assisted by the structural information extracted from π-stacked C_3-trimer models of **T3C4** and **TB3C4** computed at the B3LYP-D3/6-31G** level (see the Supporting Information for further details), larger supramolecular aggregates (decamers) of **T3C4** and **TB3C4** were constructed and optimized (Figure 2) at the tight-binding density functional theory (DFTB3) level coupled to the Grimme's -D3 dispersion correction (DFTB3-D3). Two different structures were predicted for the **T3C4** decamer at DFTB3-D3. The first optimized structure corresponds to a helical-like aggregate, in which adjacent molecules are disposed in a parallel fashion along the stacking axis and are rotated by angles in the 4−15° range (Figure 2a). The molecular units are slightly displaced in a zigzag manner with short π–π contacts around 3.4−3.6 Å. In contrast, the second optimized structure of the **T3C4** decamer shows an ellipsoid-like structure with significant folding of almost all the molecules forming the aggregate (Figure 2b). Despite its highly distorted structure, this second decamer presents some reminiscences of the helical-like structure obtained for the first decamer and for the DFT-optimized **T3C4** trimer (Figure 2a and Figure S3a). The dihedral angles (D_1 and D_2) previously used to characterize the molecular structure (Figure 1) exhibit values within a wide range due to the significant conformational disorder. Despite the disordered aspect of the aggregate, the structure predicted for the decamer still allows for favorable π–π interactions between the triazine, triazole and benzene rings with intermolecular contacts in the 3.2–4.5 Å range (Figure 2c). In fact, this distorted ellipsoid-like decamer is found to be more stable by 36.6 kcal/mol than the helical-like **T3C4** decamer.

For **TB3C4**, two stable decamer structures were also found. The first structure (Figure 2d) exhibits a helical-like aggregation mode mainly driven by π–π interactions with short intermolecular contacts between adjacent triazine units (~3.4–3.6 Å),

WILEY-VCH

triazole rings (~3.6 Å) and benzenes (~3.6 Å). This decamer presents a relatively small conformational disorder with extended arms and values for the representative dihedral angles D_1, D_2 and D_3 in the same range as those obtained for the isolated molecule. The second structure also corresponds to a helical-like aggregate (Figure 2e), but in this case the **TB3C4** monomers are slightly displaced along the stack. This **TB3C4** decamer resembles the trimer previously calculated at the B3LYP-D3/6-31G** level (Figure S3b) and is predicted to be 55.3 kcal/mol more stable than the decamer shown in Figure 2d. The slight shift of adjacent molecules along the stack, together with the high value of the twisting angle D_1 (~22°) found for one of the molecular arms, determines that two among the three arms become close and efficiently interact. In addition to the π–π interactions between the aromatic rings in the 3.8–4.6 Å range, complementary CH–π interactions are also present between the terminal alkyl chains and benzene rings.

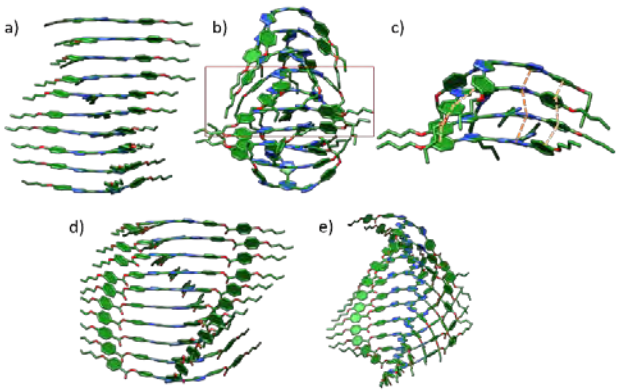

Figure 2. a-b) DFTB3-D3-optimized decamer structures calculated for **T3C4**. (c) Magnification of the central four molecules of the optimized decamer of **T3C4** shown in (b) to better visualize the intermolecular interactions. d-e) Helical-like DFTB3-D3-optimized decamers computed for **TB3C4**. Hydrogen atoms have been omitted for clarity.

DFTB3-D3 calculations therefore predict stable supramolecular aggregates for both **T3C4** and **TB3C4** governed by weak intermolecular π–π and CH–π interactions between the aromatic rings of the TTT core and also between the peripheral butoxyphenyl (**T3C4**) and butoxybenzoyloxyphenyl (**TB3C4**) groups. Interestingly, calculations suggest that **T3C4** and **TB3C4** give rise, despite their similar molecular structure, to significantly different supramolecular assemblies. The more extended peripheral groups present in **TB3C4** promote the formation of stable helical-type structures.

2.3. Preparation of nanostructures and morphological characterization

Encouraged by theoretical calculations that indicate energetically favored aggregation for both compounds with different structure, we explored the possibilities of controlling the formation of nanostructures.

It is well known that π-stacking causes the upfield shifting of the NMR signals due to the mutual shielding of the aromatic rings.[29–32] Accordingly, a concentration-dependent ^{1}H-NMR study in chloroform was carried out as a first step to explore this possibility. ^{1}H-NMR spectra of **T3C4** and **TB3C4** in $CDCl_3$ at different concentrations (5×10^{-4}, 2.5×10^{-3} and 1×10^{-1} M) were recorded (Figure 3). On increasing the concentration from 5×10^{-4} to 2.5×10^{-3} M, no changes were observed in the ^{1}H-NMR signals, suggesting that this concentration is still too low for aggregation. Nevertheless, when the concentration was increased up to 1×10^{-1} M, both the aromatic and the triazole protons of **T3C4** and **TB3C4** shifted upfield. This is in agreement with the short distances (3.5–3.9 Å) computed for the π-stacked trimer and decamer models (Figure S3 and Figure 2), and confirms that both compounds are able to self-assemble in chloroform above this concentration. The upfield shifting is more pronounced for **TB3C4**, probably due to the presence of an additional aromatic benzoyloxy moiety, which makes more effective the interactions between the π-systems of adjacent

molecules in the aggregate. In the case of **TB3C4**, a widening of proton signals was also observed resulting in a loss of resolution of the signals, additionally endorsing the aggregation.[29] Based on the behavior observed in the ^{1}H-NMR spectra, transmission electron microscopy (TEM) images were taken for samples of **T3C4** and **TB3C4** at 1×10^{-1} M in $CDCl_3$ (Figure S4) revealing the formation of spherical nanoparticles in both cases, with sizes ranging from 200 to 1200 nm for **T3C4** and from 500 to 1000 nm in the case of **TB3C4**.

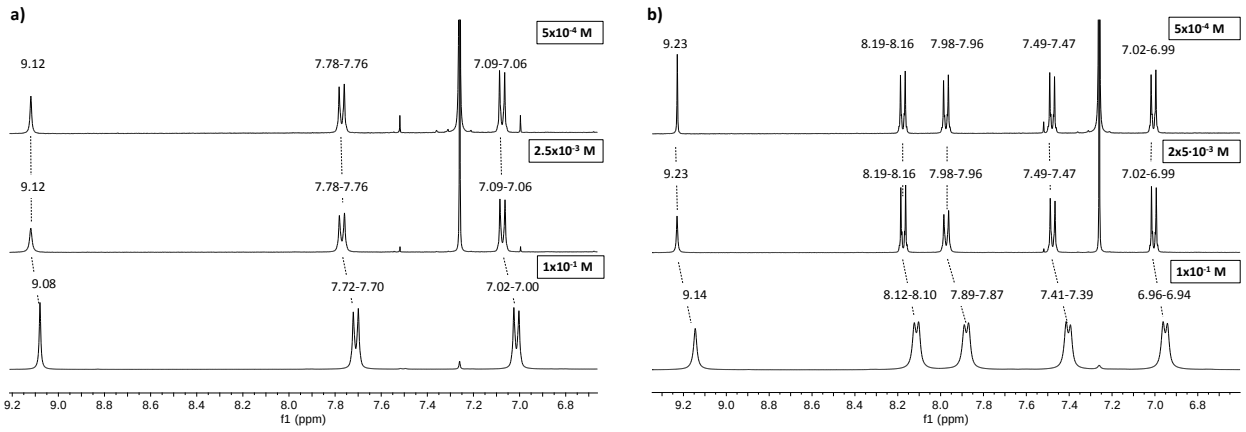

Figure 3. ^{1}H-NMR spectra (aromatic region) of **T3C4** (a) and **TB3C4** (b) in $CDCl_3$ at different concentrations.

To achieve fine control of the nanostructure size and morphology, we proposed the use of the reprecipitation method, which consists on a rapid mixing of a small volume of a concentrated solution of the organic compound with a miscible mixture of a good solvent and a non-solvent (See the Supporting Information).[1] Thus, the molecules are quickly exposed to the presence of the non-solvent, causing the growth of the aggregates. This experimental procedure has been widely used for obtaining nanomaterials from organic molecules owing to its simplicity and versatility.[12,33] Moreover, reprecipitation has been employed as a method to control the morphology of

WILEY-VCH

the so-obtained nanostructures.[34] In this work, two different solvent/non-solvent pairs were used, i.e. $CHCl_3$/MeOH and THF/H_2O.

T3C4 formed aggregates in both $CHCl_3$/MeOH and THF/H_2O mixtures. TEM and scanning electron microscopy (SEM) images from samples in $CHCl_3$/MeOH revealed the formation of single-hollow spheres (Figure 4a-d). This morphology is quite rare for small organic molecules.[35,36] The aggregates appeared to be more defined when the amount of MeOH was above 50%. In addition, the size of the nanoparticles varied with the amount of non-solvent in the mixture: for samples with lower MeOH ratio (50%), aggregates of 60–150 nm were observed, whereas when the non-solvent ratio was increased to 70%, the particles grew up to 150–250 nm. In a similar way, **T3C4** aggregated in THF/H_2O mixtures at high water ratios. Above a 60% of water, well-defined single-hole hollow nanospheres with sizes ranging from 70 to 250 nm were formed as confirmed by SEM and TEM (Figure 4e-h). In TEM images, a round shell could be observed inside the nanosphere, indicating that they were hollow.

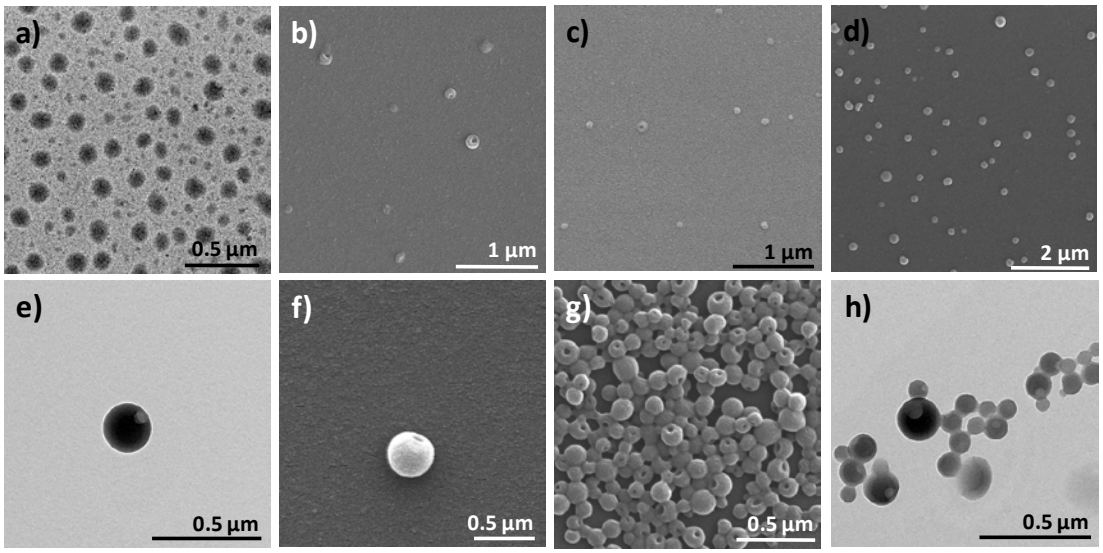

Figure 4. SEM (b, c, d, f and g) and TEM (a, e and h) images of **T3C4** aggregates in $CHCl_3$/MeOH 50/50 (a, b), $CHCl_3$/MeOH 40/60 (c), $CHCl_3$/MeOH 30/70 (d), THF/H_2O 30/70 (e, f) and THF/H_2O 10/90 (g, h) mixtures.

For **TB3C4** in $CHCl_3$/MeOH mixtures, the amount of non-solvent in the solution strongly influenced the self-assembly process, giving rise to a variety of morphologies for the solvent mixtures containing 30% MeOH or higher. For the solvent mixture containing 30% of MeOH, spherical and toroid-like aggregates were detected, as well as other intermediate structures such as Y-junctions, lariats or eights formed by two adjacent toroids (Figure 5a). These type of incomplete architectures, derived from the toroids, are commonly found when toroidal structures are formed.[37] It is remarkable that hollow nanostructures such as one-hole spheres or toroids were obtained for both **T3C4** and **TB3C4**. These kind of nanostructures, unlike spheres or wires, are not so commonly detected because the range of solvent/non-solvent ratio in which they are stable is usually narrow. In the literature, toroids were normally described for amphiphilic polymers, dumbbell-shaped molecules or biological macromolecules (DNA or biopolymers),[37–41] and recently they have been also reported for small organic molecules.[16,42]

When the amount of MeOH in the mixture was incremented, a drastic change in the morphology of the aggregates occurred, and the formation of twisted fibers of increasing size was observed. Firstly, short wires of 300–500 nm where observed when the amount of MeOH was 40% (Figure 5b-c). Further increase to 50–90% of MeOH yielded longer fibers of several micrometer length (Figure 5d-f). These long fibers twisted forming screws, "phone cord-like" structures or helical nanotubes, scarcely reported in self-assembly systems from achiral molecules,[15] as clearly revealed both SEM and TEM images. Occasionally, they closed on themselves giving rise to rings or entwined with other fibers in rope-like structures.

10.1002/cnma.201800484

WILEY-VCH

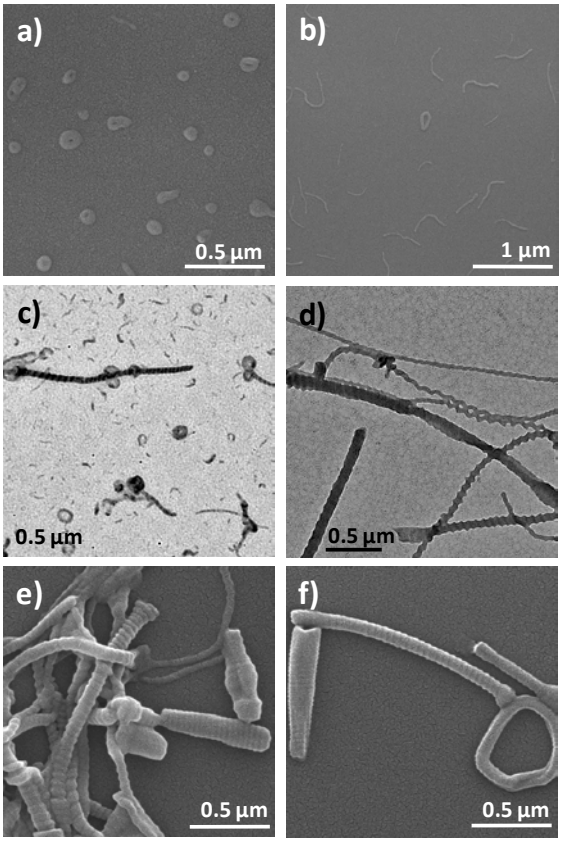

Figure 5. SEM (a, b, e and f) and TEM (c and d) images of **TB3C4** aggregates in $CHCl_3$/MeOH 70/30 (a), $CHCl_3$/MeOH 60/40 (b, c) and $CHCl_3$/MeOH 20/80 (d, e, f) mixtures.

When the mixture of solvents was THF/H_2O, aggregates were observed for water concentrations equal or above 60%. As shown in TEM and SEM, the solvent mixture containing 60% of water allowed the formation of nanospheres of sizes ranging from 60 to 120 nm (Figure 6a-b). The increase of the amount of water in the mixture expanded the formation of the same particles (around 60 nm in size). Finally, when the concentration of water was augmented to 90%, a large network of smaller spheres (40–60 nm) was observed (Figure 6c-d). Hence, in this case, the increase of the non-solvent in the mixture did not cause significant morphology changes compared to the $CHCl_3$/MeOH solvent mixture.

WILEY-VCH

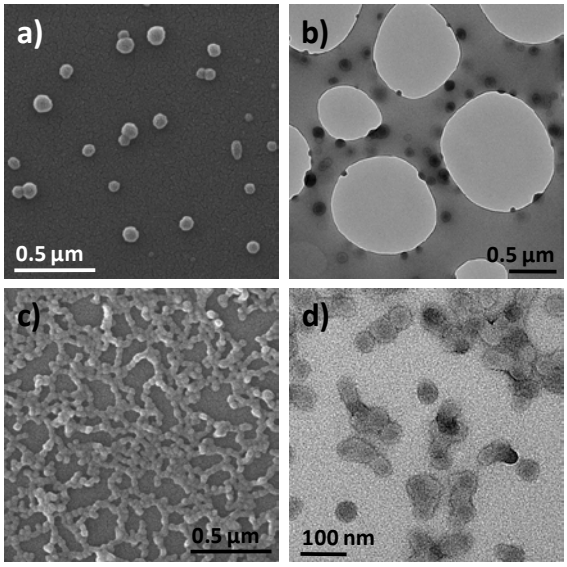

Figure 6. SEM (a and c) and TEM (b and d) images of **TB3C4** aggregates in THF/H_2O 40/60 (a, b) and THF/H_2O 10/90 (c, d) mixtures.

Experimental results can be tentatively related to B3LYP-D3 and DFTB3-D3 calculations that predicted different aggregation processes for **T3C4** and **TB3C4**. **T3C4**, owing to the favored folding of the molecular units (Figure 2b), may give rise to more rounded supramolecular assemblies, in line with the nanospheres observed in both solvent systems. In contrast, for **TB3C4** more ordered and extended aggregates were calculated (Figure 2d and e), which could make more easy the interaction with their surroundings, i.e. solvent molecules and vicinal aggregates. This may support the different aggregates experimentally observed for **TB3C4** depending on the solvent system, forming wires, helical nanotubes or Y-junction nanoforms for the $CHCl_3$/MeOH system and spherical objects in THF/H_2O.

In light of the well-defined nanostructures observed by TEM and SEM, ^{1}H-NMR experiments at different $CDCl_3$/CD_3OD and THF-d8/D_2O ratios were performed for **T3C4** (Figure S5) and **TB3C4** (Figure 7) to bring additional data to understand the self-assembly process. Samples were prepared at a constant concentration of 1×10^{-4} M and tetrakis(trimethylsilyl)silane was employed as a chemical-shift standard. Figure 7

WILEY-VCH

gathers the ^{1}H-NMR spectra recorded for **TB3C$_4$** dissolved in each solvent mixture at four different solvent/non-solvent ratios. Interestingly, upon the addition of a small amount of the non-solvent, i.e. 20%, a drastic intensity reduction is observed for all the signals indicating the decrease of molecularly dissolved **TB3C$_4$** due to the self-assembly process. In addition, a significant down-field shift of the triazole proton (from 9.22 to 9.71 ppm in $CDCl_3$/ CD_3OD and from 9.62 to 9.91 ppm in THF-d8/D_2O) is observed, likely due to interaction with the protic non-solvent. Further increase of the relative amount of the non-solvent, CD_3OD or D_2O, provokes the formation of assemblies that are NMR-silent, revealing the formation of solid-like nano-objects and confirming the presence of nanoaggregates in solution. This effect occurs at lower amount of the non-solvent for the mixture THF-d8/D_2O.

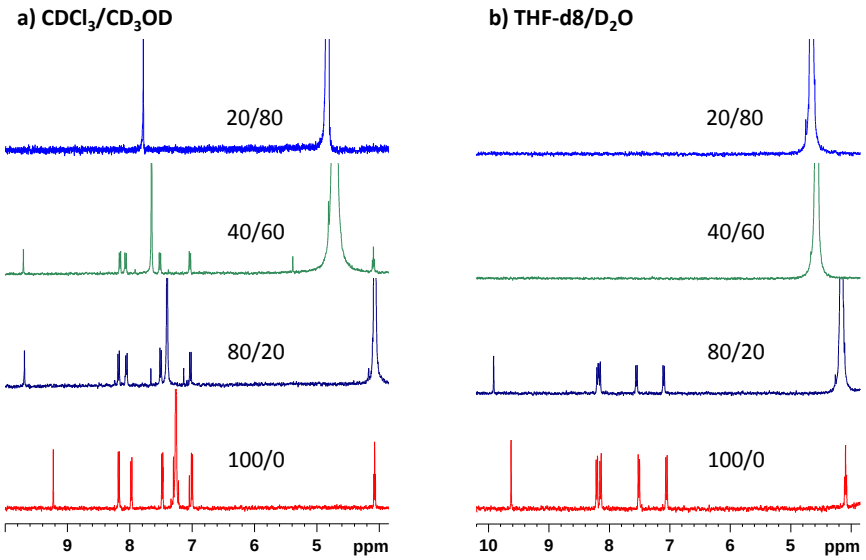

Figure 7. ^{1}H NMR spectra recorded for **TB3C$_4$** dissolved in solvent/non-solvent mixtures at different ratios and a concentration of 1×10^{-4} M. a) $CDCl_3$/CD_3OD and b) THF-d8/D_2O.

2.4. Optical properties of T3C$_4$ and TB3C$_4$ aggregates

Aggregation of optically active organic molecules has been shown to have a great influence in their photophysical features. Hence, the absorption and emission

spectra of **T3C4** and **TB3C4** were recorded in different solvent/non-solvent mixtures to investigate the possible changes caused in the optical properties by the formation of different nanostructures.

T3C4 is fluorescent in solution, exhibiting an emission band at 416 nm in $CHCl_3$ with a quantum yield of 0.57 (Figure S6). However, the aggregation process caused by adding methanol produces a quenching of the emission. The same occurs for the THF/H_2O mixtures (Figure S7 and S8).

In contrast, **TB3C4** shows a weak fluorescence band in $CHCl_3$ (λ_{em} = 385 nm) or THF (λ_{em} = 379 nm), which increases in the solvent mixtures containing aggregates (Figure S9). The plot in Figure 8a represents the dependence of the ratio I/I_0 (I = fluorescence intensity measured at the different solvent/non-solvent mixtures; I_0 = fluorescence intensity in pure $CHCl_3$ solution) vs the percentage of MeOH in the solvent mixture. The fluorescence intensity (I) increased up to 7 times for the sample containing a 40 % of MeOH in comparison with the compound dissolved in $CHCl_3$ (I_0). Surprisingly, higher percentage of MeOH caused the emission to decrease again reaching a minimum for the sample containing 70% MeOH. The drop in emission coincides with a change in the morphology of the aggregates. Indeed, over 40% MeOH, the spherical and toroidal aggregates disappeared, leading to the formation of short twisted fibers, which evolved to phone-cord like fibers and helical nanotubes of a few microns while increasing the amount of non-solvent. Thereby, aggregation of **TB3C4** in $CHCl_3$/MeOH represents a new example of a compound with tuneable optical properties by means of control on the aggregation process.

More significant is the emission increase shown by **TB3C4** when THF/H_2O mixtures are used. As depicted in Figure 8b, the fluorescence intensity of **TB3C4** reached a maximum for the mixture containing an 80% of water. For this sample, the emission intensity (I) was more than 60 times higher than that of the solution in pure

WILEY-VCH

THF (I_0), a value much greater than the obtained in the $CHCl_3$/MeOH mixtures. An intense emission was also observed after removing the solvent for the dry sample (Figure S10). Anew, the influence of the morphology of the aggregates on the variation of the fluorescence was proven, since the mixture containing 90% of water again showed a slight decrease in the emission intensity, probably due to the formation of a less stable 3D-network of smaller spherical aggregates. **TB3C4** therefore constitutes an interesting example of a compound that exhibits an enhancement of the emission by nanoparticle formation.

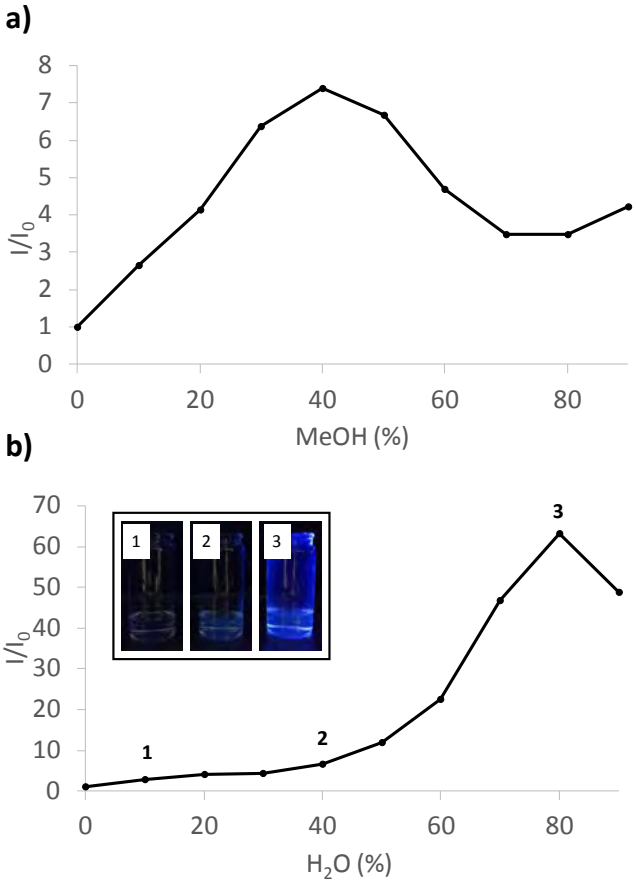

Figure 8. Fluorescence intensity ratio (I/I_0) as a function of the percentage of non-solvent for **TB3C4** in $CHCl_3$/MeOH (a) and THF/H_2O (b) mixtures.

It has been therefore observed that the optical properties of **T3C4** and **TB3C4** vary from those of the compounds molecularly dissolved when aggregates are obtained by using the reprecipitation method. Additionally, **T3C4** and **TB3C4** show different performances in terms of how aggregation affects the emission. One factor could be related to the different emitting properties of the non-aggregated **T3C4** and **TB3C4** compounds in solution; that is, **T3C4** is fluorescent whereas **TB3C4** hardly emits despite having the same emitting moiety: the TTT core. The structural difference is the presence of an extra benzoyloxy moiety, which adds flexibility to the molecule and could favor non-radiative deactivation channels leading to low emission efficiency. However, this deactivation pathway should be less favored when **TB3C4** is in the aggregated state due to the rigid environment that could restrict the internal rotation, similar to what it has been postulated for other AIE molecules.[20]

To explore in more detail the intramolecular factors involved in the emission enhancement of **TB3C4**, relaxed torsion potentials of the most representative dihedral angles between the different aromatic rings were first calculated for the **TB3C4** compound at the B3LYP-D3/6-31G** level. Figure 9 reveals that the rotation between the triazine and the triazole units (dihedral angle D_1) is highly hindered, due to the disruption of the electronic conjugation between these rings, with an energy barrier of 9.1 kcal/mol.

The rotation around the dihedral angle D_2 (between the triazole and the benzene rings) is less impeded with barriers below 3.0 kcal/mol. Importantly, the softest torsion potential is obtained for the dihedral angle D_3 between the inner benzene and the benzoyloxy moiety with energy barriers of ca. 1.0 kcal/mol. The benzoyloxy groups therefore rotate almost freely at room temperature ($k_BT \sim 0.6$ kcal/mol), and this rotation may represent a favorable mechanism for energy dissipation in the low-lying

WILEY-VCH

electronic excited states. This would explain the fluorescence quenching of **TB3C4** in solution, which presents a very low fluorescence quantum yield.

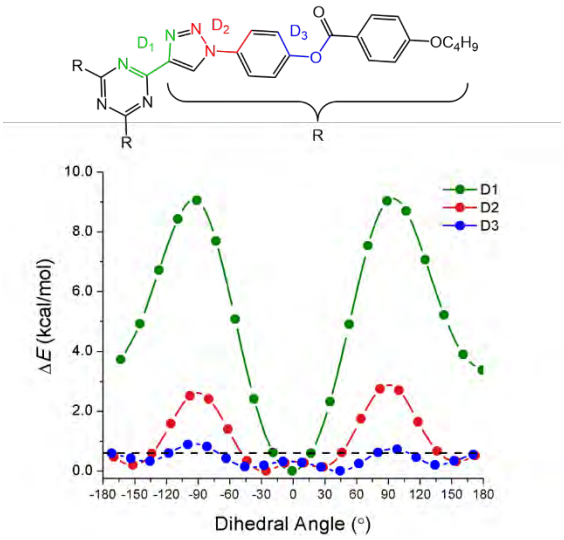

Figure 9. Relaxed torsion potentials calculated for selected dihedral angles (D_1, D_2 and D_3) of **TB3C4** at the B3LYP-D3/6-31G** level. The horizontal dashed black line indicates k_BT energy at room temperature (~ 0.6 kcal/mol).

In a second step, singlet excited states were computed from single-point time-dependent DFT calculations (TDDFT) on the different relaxed structures obtained along the torsional D_3 scan at B3LYP-D3/6-31G**. Figure 10 displays the excitation energies obtained for the first five singlet excited states (S_1 to S_5) of **TB3C4**. The internal rotation involving the D_3 angle gives rise to crossing between the low-lying excited states (particularly between the first three excited states) opening the door for dissipation pathways. For the molecular aggregates of **TB3C4**, the dihedral angle D_3 is calculated to be in the 28–40° range and the rotation of the benzoyloxy groups is hindered by the proximity of the adjacent molecules. In the 28–40° interval of D_3 values, the first singlet excited state for **TB3C4** is a bright state with a high oscillator strength (Figure 10). This state would be therefore responsible for the enhanced

WILEY-VCH

fluorescence emission observed experimentally due to the restriction of the torsion freedom. The restriction of intramolecular motions (in particular, hindered low-frequency torsions) is the most common invoked mechanism to successfully explain the AIE phenomenon.[19] This mechanism has been theoretically corroborated in molecular cluster models where the estimated non-radiative rate constants turned out to be smaller than those computed for the isolated systems.[43–45]

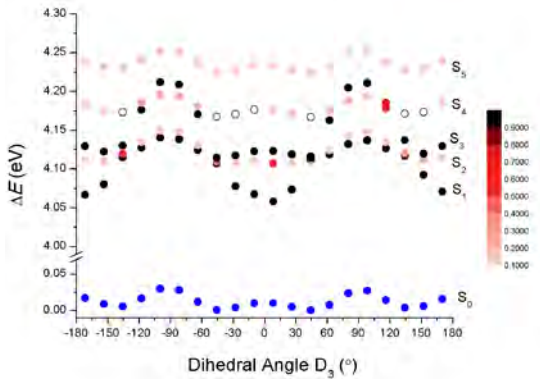

Figure 10. B3LYP-D3/6-31G** excitation energies calculated for the five lowest-lying singlet excited states (S_n) of **TB3C4** as a function of the dihedral angle D_3. The colour of the energy points represents the value of the oscillator strength as indicated on the scale on the right. Ground state (S_0) energies in blue have been included for comparison purposes.

Our theoretical outcomes therefore highlight that, in the isolated **TB3C4** compound, the torsion of the terminal benzoyloxy moieties has almost no energy cost at room temperature and, thus, is likely to be an efficient mechanism for fluorescence quenching. Singlet excited state calculations show that crossings between the low-lying excited states are expected through this rotation, giving rise to accessible non-radiative pathways. The restriction of the torsional motion in the molecular aggregates obstructs the energy-dissipating pathways and explains satisfactorily why **TB3C4** exhibits enhanced emission in the molecular assemblies.

3. Conclusions

This work reports on the use of the straightforward reprecipitation method to precisely control the morphology during the preparation of nanostructures from two non-amphiphilic star-shape 2,4,6-tris(1,2,3-triazol-4-yl)-1,3,5-triazines (**T3C$_4$** and **TB3C$_4$**). Simple variations in some preparation parameters, such as the selection of the solvent/non-solvent pair or the relative amount of both solvents, lead to a variety of exciting architectures such as spherical particles, one-hole hollow spheres, toroids, twisted fibers or helical nanotubes.

The two derivatives allowed the study of the effect of the chemical structure on the aggregation and the optical properties. Compared to **T3C$_4$**, the introduction of an additional benzoyloxy moiety with the ability to rotate in **TB3C$_4$** completely changed the emissive behavior. Whereas **T3C$_4$** acted as a conventional fluorescent molecule, in which aggregation caused the quenching of the emissive properties, **TB3C$_4$** represented an example of a molecule that exhibits enhancement of the emission upon aggregation. The control of the solvent/non-solvent mixture and thereby the morphology of the aggregate has been revealed as a tool for tuning the emission properties.

Conflicts of interest

There are no conflicts to declare.

Acknowledgement

This work was financially supported by the MINECO-FEDER (UE) funds (projects MAT2015-66208-C3-1, CTQ2015-71154-P, and Unidad de Excelencia María de Maeztu MDM-2015-0538), the Generalitat Valenciana (PROMETEO/2016/135 and SEJI/2018/035), the Gobierno de Aragón-FSE (UE) (E47_17R) and PI2 program from

ICMA-CSIC, M.C. and J.C. are grateful to the MINECO for their predoctoral contracts. J.A. is also thankful to the MINECO for a "JdC-Incorporación" Fellowship (IJCI-2015-26154). We would like to acknowledge the use of "Servicios Científico-Técnicos" of CEQMA (UZ-CSIC), Servicio General de Apoyo a la Investigación – SAI, Universidad de Zaragoza, and the Laboratory of Advanced Microscopies, LMA-INA, Universidad de Zaragoza.

[1] Y. S. Zhao, H. Fu, A. Peng, Y. Ma, D. Xiao, J. Yao, *Adv. Mater.* **2008**, *20*, 2859.

[2] E. Busseron, Y. Ruff, E. Moulin, N. Giuseppone, *Nanoscale* **2013**, *5*, 7098.

[3] Y. Yan, Y. S. Zhao, *Chem. Soc. Rev.* **2014**, *43*, 4325.

[4] D. Yan, *Chem. - A Eur. J.* **2015**, *21*, 4880.

[5] D. Jiang, Z. Xue, Y. Li, H. Liu, W. Yang, *J. Mater. Chem. C* **2013**, *1*, 5694.

[6] S. Chen, Z. Qin, T. Liu, X. Wu, Y. Li, H. Liu, Y. Song, Y. Li, *Phys. Chem. Chem. Phys.* **2013**, *15*, 12660.

[7] F. Tang, C. Wang, J. Wang, X. Wang, L. Li, *ACS Appl. Mater. Interfaces* **2014**, *6*, 18337.

[8] M. Hasegawa, M. Iyoda, *Chem. Soc. Rev.* **2010**, *39*, 2420.

[9] S. Kundu, A. Patra, *Chem. Rev.* **2017**, *117*, 712.

[10] M. Abyan, D. De Caro, S. Fery-Forgues, *Langmuir* **2009**, *25*, 1651.

[11] S. P. Anthony, S. M. Draper, *J. Phys. Chem. C* **2010**, *114*, 11708.

[12] Y. Luo, Z. Xue, Y. Li, H. Liu, W. Yang, Y. Li, *RSC Adv.* **2015**, *5*, 100457.

[13] L. Maggini, D. Bonifazi, *Chem. Soc. Rev.* **2012**, *41*, 211.

[14] M. Martínez-Abadía, R. Giménez, M. B. Ros, *Adv. Mater.* **2017**, *1704161*.

[15] Y. Sang, P. Duan, M. Liu, *Chem. Commun.* **2018**, *54*, 4025.

[16] X. Jin, D. Yang, Y. Jiang, P. Duan, M. Liu, *Chem. Commun.* **2018**, *54*, 4513.

[17] B. K. An, S. K. Kwon, S. D. Jung, S. Y. Park, *J. Am. Chem. Soc.* **2002**, *124*, 14410.

[18] J. Luo, Z. Xie, J. W. Y. Lam, L. Cheng, B. Z. Tang, H. Chen, C. Qiu, H. S. Kwok, X. Zhan, Y. Liu, D. Zhu, *Chem. Commun.* **2001**, *381*, 1740.

[19] J. Mei, Y. Hong, J. W. Y. Lam, A. Qin, Y. Tang, B. Z. Tang, *Adv. Mater.* **2014**, *26*, 5429.

[20] J. Mei, N. L. C. Leung, R. T. K. Kwok, J. W. Y. Lam, B. Z. Tang, *Chem. Rev.* **2015**, *115*, 11718.

[21] J. Shi, L. E. Aguilar Suarez, S. J. Yoon, S. Varghese, C. Serpa, S. Y. Park, L. Lüer, D. Roca-Sanjuán, B. Milián-Medina, J. Gierschner, *J. Chem. Phys.* **2017**, *121*, 23166.

[22] E. Beltrán, J. L. Serrano, T. Sierra, R. Giménez, *Org. Lett.* **2010**, *12*, 1404.

[23] E. Beltrán, J. L. Serrano, T. Sierra, R. Giménez, *J. Mater. Chem.* **2012**, *22*, 7797.

[24] E. Beltrán, M. Garzoni, B. Feringán, A. Vancheri, J. Barberá, J. L. Serrano, G. M. Pavan, R. Giménez, T. Sierra, *Chem. Commun.* **2015**, *51*, 1811.

[25] B. Feringán, P. Romero, J. L. Serrano, R. Giménez, T. Sierra, *Chem. - A Eur. J.* **2015**, *21*, 8859.

[26] B. Feringán, P. Romero, J. L. Serrano, C. L. Folcia, J. Etxebarria, J. Ortega, R. Termine, A. Golemme, R. Giménez, T. Sierra, *J. Am. Chem. Soc.* **2016**, *138*, 12511.

[27] S. I. Kato, S. Jin, T. Kimura, N. Yoshikawa, D. Nara, K. Imamura, Y. Shiota, K. Yoshizawa, R. Katoono, T. Yamanobe, H. Uehara, Y. Nakamura, *Org. Biomol. Chem.* **2018**, *16*, 3584.

[28] C. Courme, S. Gillon, N. Gresh, M. Vidal, C. Garbay, J. C. Florent, E. Bertounesque, *Tetrahedron Lett.* **2008**, *49*, 4542.

[29] G. Fernández, E. M. Pérez, L. Sánchez, N. Martín, *Angew. Chemie - Int. Ed.* **2008**, *47*, 1094.

[30] A. Pérez, D. De Saá, A. Ballesteros, J. L. Serrano, T. Sierra, P. Romero, *Chem. - A Eur. J.* **2013**, *19*, 10271.

[31] C. Zhang, C. Yu, H. Long, R. J. Denman, Y. Jin, W. Zhang, *Chem. - A Eur. J.* **2015**, *21*,

16935.

[32] Y. Takaki, R. Ozawa, T. Kajitani, T. Fukushima, M. Mitsui, K. Kobayashi, *Chem. - A Eur. J.* **2016**, *22*, 16760.

[33] M. Yang, P. Xing, M. Ma, Y. Zhang, Y. Wang, A. Hao, *Soft Matter* **2016**, *12*, 6038.

[34] K. Kazlauskas, G. Kreiza, E. Arbačiauskienė, A. Bieliauskas, V. Getautis, A. Šačkus, S. Juršėnas, *J. Phys. Chem. C* **2014**, *118*, 25261.

[35] D. M. Li, Y. S. Zheng, *J. Org. Chem.* **2011**, *76*, 1100.

[36] Q. Li, H. Ma, Y. Jia, J. Li, B. Zhu, *Chem. Commun.* **2015**, *51*, 7219.

[37] D. J. Pochan, Z. Chen, H. Cui, K. Hales, K. Qi, K. L. Wooley, *Science (80-.).* **2004**, *306*, 94.

[38] Z. Chen, H. Cui, K. Hales, Z. Li, K. Qi, D. J. Pochan, K. L. Wooley, *J. Am. Chem. Soc.* **2005**, *127*, 8592.

[39] J. K. Kim, E. Lee, Z. Huang, M. Lee, *J. Am. Chem. Soc.* **2006**, *128*, 14022.

[40] E. Lee, Y. H. Jeong, J. K. Kim, M. Lee, *Macromolecules* **2007**, *40*, 8355.

[41] Y. B. Lim, E. Lee, M. Lee, *Macromol. Rapid Commun.* **2011**, *32*, 191.

[42] J. Cai, J. Liu, T. Wang, J. Wang, L. Jiang, *J. Mater. Chem. C* **2018**, *6*, 3849.

[43] Q. Peng, Y. Yi, Z. Shuai, J. Shao, *J. Am. Chem. Soc.* **2007**, *129*, 9333.

[44] Q. Wu, Q. Peng, Y. Niu, X. Gao, Z. Shuai, *J. Phys. Chem. A* **2012**, *116*, 3881.

[45] Q. Wu, C. Deng, Q. Peng, Y. Niu, Z. Shuai, *J. Comput. Chem.* **2012**, *33*, 1862.

10.1002/cnma.201800484

WILEY-VCH

The table of contents entry

Non-amphiphilic achiral star-shaped triazines self-assemble into hollow spheres, twisted fibres or phone cord-like helical nanotubes just by following a straightforward reprecipitation method. Control of the self-assembly morphologies and photoluminescent properties can be achieved, and aggregation induced emission is observed.

Self-assembly

Martín Castillo-Vallés, Eduardo Beltrán, Jesús Cerdá, Juan Aragó, Pilar Romero, José Luis Serrano, Enrique Ortí, Raquel Giménez* and Teresa Sierra**

Self-assembly of clicked star-shaped triazines into functional nanostructures

ToC figure